Single Molecule Nanospectroscopy Visualizes Proton-Transfer Processes within a Zeolite Crystal
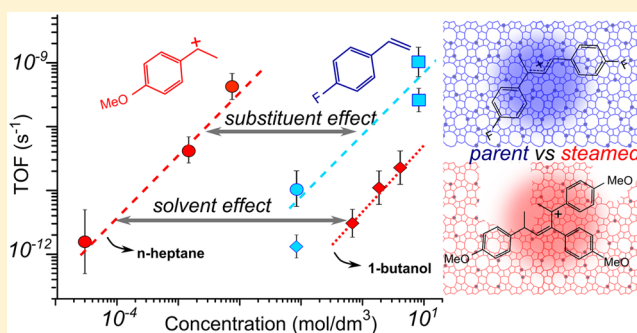
Zoran Ristanović,[†] Alexey V. Kubarev,[‡] Johan Hofkens,[§] Maarten B. J. Roeffaers,*[‡] and Bert M. Weckhuysen*[†]

[†]Inorganic Chemistry and Catalysis, Utrecht University, Universiteitsweg 99, 3584 CG Utrecht, The Netherlands
[‡]Centre for Surface Chemistry and Catalysis and [§]Department of Chemistry, KU Leuven, Celestijnenlaan 200 F, 3001 Heverlee, Belgium

ⓢ Supporting Information

ABSTRACT: Visualizing proton-transfer processes at the nanoscale is essential for understanding the reactivity of zeolite-based catalyst materials. In this work, the Brønsted-acid-catalyzed oligomerization of styrene derivatives was used for the first time as a single molecule probe reaction to study the reactivity of individual zeolite H-ZSM-5 crystals in different zeolite framework, reactant and solvent environments. This was accomplished via the formation of distinct dimeric and trimeric fluorescent carbocations, characterized by their different photostability, as detected by single molecule fluorescence microscopy. The oligomerization kinetics turned out to be very sensitive to the reaction conditions and the presence of the local structural defects in zeolite H-ZSM-5 crystals. The remarkably photostable trimeric carbocations were found to be formed predominantly near defect-rich crystalline regions. This spectroscopic marker offers clear prospects for nanoscale quality control of zeolite-based materials. Interestingly, replacing *n*-heptane with 1-butanol as a solvent led to a reactivity decrease of several orders and shorter survival times of fluorescent products due to the strong chemisorption of 1-butanol onto the Brønsted acid sites. A similar effect was achieved by changing the electrophilic character of the *para*-substituent of the styrene moiety. Based on the measured turnover rates we have established a quantitative, single turnover approach to evaluate substituent and solvent effects on the reactivity of individual zeolite H-ZSM-5 crystals.

■ INTRODUCTION

Zeolites are microporous aluminosilicates that are heavily used as solid acid catalysts due to the unique combination of acidic and shape-selective properties.[1,2] In particular, zeolites are of high importance in catalytic processes in the petrochemical industry. More recently, they are also considered to be implemented in future biorefineries.[3−8] A challenge in the rational design of zeolite-based catalysts is to control the number, distribution and nature of (Brønsted) acid sites. Significant progress has been made recently in the direction of tailoring hierarchical zeolite catalysts with remarkably improved catalytic activity, selectivity, and stability.[9,10]

Understanding the synergy between the numerous physicochemical processes taking place in zeolite-based catalysts demands for fundamental insights into the host−guest interactions, preferably at the single particle−single molecule level. Porosity, crystalline defects of the catalyst, guest mobility, as well as solvent effects, can strongly interfere with Brønsted acid-catalyzed processes taking place within zeolite catalysts. Nowadays, there is a tendency to perform catalytic reactions in the liquid phase leading to an abundance of various organic guest molecules that influence the proton-transfer processes taking place within the cages and channels of zeolites. Finally,

recent characterization studies at the single particle level emphasize the importance of the underlying structural differences between individual zeolite particles where surface diffusion barriers and crystalline defects may play an important role.[11−17]

It should be evident that the chemical nature of the above-described processes at the solid−liquid interface of zeolites is poorly studied at the single particle level and relevant time and length scales, partially due to the insensitivity and ensemble averaging nature of traditionally used spectroscopic methods. Consequently, spatially resolved information about the accessibility of Brønsted acid sites and the real-time changes in reactivity of a single zeolite particle cannot be visualized by these bulk characterization methods.[12,18] To overcome this limitation, several techniques based on optical microscopy methods have been developed in recent years for the study of Brønsted acid-catalyzed reactions at the single particle level.[19−21] Hence, selective staining of zeolite acid sites[22] is becoming a popular strategy to study Brønsted reactivity of zeolite particles where fluorescent species are generated after an

acid catalyzed conversion of molecules, such as furfuryl alcohol,[23−26] thiophene,[27] and styrene.[28−30]

After the great success in life sciences,[31] single molecule fluorescence microscopy has become a powerful and sensitive tool to study chemistry, physics and materials science at the molecular scale. The localization of fluorescent emitters leads to the spatiotemporal resolutions in the orders of 10 nm and 10 ms, provided that the fluorescent species possess sufficient brightness and photostability. Several excellent reviews highlight the high relevance of the single molecule fluorescence approach in many fields of chemistry.[19,32−38] The broad scope of single molecule fluorescence microscopy includes studies of kinetics and mechanisms of stoichiometric chemical reactions,[39,40] collisions of conjugated polymers in liquid phase,[41] distribution and transport of charge carriers in semiconductors,[42,43] diffusion in porous materials,[44,45] localization of plasmonic hotspots,[46,47] and single-turnover kinetics of solid catalysts.[24−26,48−53]

Among the above-mentioned fluorogenic reactions, the Brønsted-acid-catalyzed oligomerization of styrene-based derivatives has received high interest due to the existence of several carbocationic species that are considered as frequently encountered reaction intermediates in zeolite chemistry.[54] Importantly, styrene and its derivatives fit inside the pores of medium and large pore zeolites and oligomerize further to generate carbocationic species that absorb and emit light in the visible region. By changing the substituents on the styrene moiety, it is possible to probe the acidic and shape-selective properties of zeolites.[29] The oligomerization reactions using 14 different styrene substituents were initially performed on large zeolite H-ZSM-5 crystals as model systems[28,29,55] and further extended to industrially relevant zeolite-based catalysts, such as fluid catalytic cracking (FCC) particles and catalyst bodies based on H-ZSM-5 and H-Y.[56−58]

In this work, we apply for the first time the Brønsted-acid-catalyzed oligomerization of styrene derivatives to study the influence of solvent polarity and defect density on the reactivity of zeolite H-ZSM-5 at the single particle—single molecule level. Using 4-methoxystyrene and 4-fluorostyrene as selective and versatile probes we showcase the importance of pore accessibility and defect chemistry for the selective formation of different reaction intermediates. To accomplish this, we have studied two types of zeolite crystals, namely, highly microporous parent zeolite H-ZSM-5 crystals and defect-rich, mildly steamed zeolite H-ZSM-5 crystals with induced mesoporosity.[26,30,59−61] Based on this study, a spectroscopic marker for nanoscale quality control of zeolite-based materials could be identified. Furthermore, we show that the single molecule oligomerization kinetics and stability of fluorescent carbocations can be further controlled by the polarity of solvent molecules.

■ EXPERIMENTAL SECTION

Zeolite Materials. Large zeolite H-ZSM-5 crystals (dimensions: $100 \times 20 \times 20 \ \mu m^3$) were used as provided by ExxonMobil (Machelen, Belgium). The synthesis has been reported elsewhere.[59,61] Tetrapropylammonium as template was removed by calcination at 823 K for 8 h (1 K/min). The crystals were subsequently converted into their acidic form by a triple ion exchange with 10 wt % ammonium nitrate (99+% Acros Organics) at 353 K, followed by 6 h calcination at 773 K. The steamed zeolite H-ZSM-5 was treated at 773 K in a water-saturated N_2 flow (150 mL/min) for 5 h. The resulting crystals were previously characterized in detail by Aramburo et al.[61]

Single Molecule Fluorescence Microscopy. An inverted epifluorescence wide-field microscope (Olympus IX-71) was used for the single molecule experiments. Both a 532 nm excitation (with a 545 nm long-pass filter) and a 561 nm excitation (a 575 nm long-pass filter) were used. The excitation light was focused by a 100× oil immersion objective lens (1.4 NA) and the emitted fluorescence light was detected by a highly sensitive electron multiplying charge-coupled device (EMCCD) camera (ImagEM Enhanced C9100-23B, Hamamatsu). The fluorescence microscopy movies were recorded with acquisition times of 30 and 100 ms per frame.
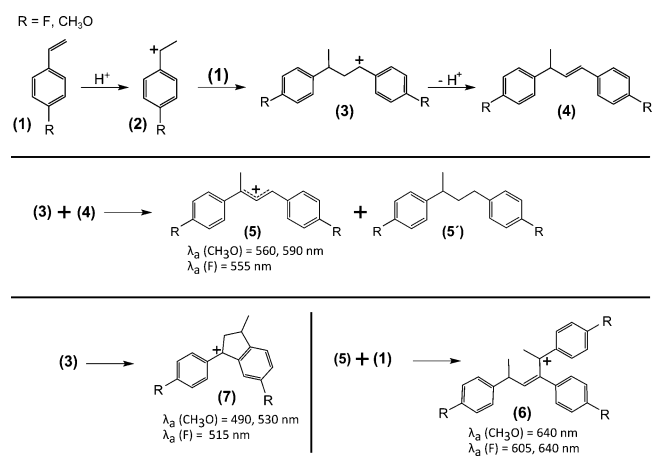
Data Analysis. The recorded single molecule fluorescence microscopy movies were analyzed with the *Localizer* software developed by Dedecker et al.[62] for *Igor Pro* (Wavemetrics) and *Matlab* (MathWorks). The localization of fluorescent events was done by independent segmentation of each frame into emissive spots and background as described by Sergé et al.[63] A list of initial emitter positions was determined with subdiffraction limited resolution by fitting a 2-D Gaussian using the Levenberg−Marquardt least-squares algorithm as implemented in the GNU Scientific Library. The emitter-tracking algorithm, as implemented in the *Localizer*, has been used for analysis of the single emitter survival.

Experiments. All single molecule fluorescence microscopy experiments were performed at room temperature. H-ZSM-5 crystals were loaded on a cover glass that was previously attached in a reactor designed for liquid-phase single molecule microscopy experiments. Typically, 1 mL of the solution containing 4-methoxystyrene or 4-fluorostyrene dissolved in either heptane (spectroscopic grade) or butanol (spectroscopic grade, vacuum distilled) was subsequently added. The reaction was then monitored by focusing at the surface of the bottom facet or by moving the focus to any provisional focal depth in the axial Z-direction up to $Z = 20 \pm 0.2 \ \mu m$. Prior to measurements, the zeolite crystals were activated at 773 K (1 K/min) for 24 h in static air to avoid residual fluorescence.

■ RESULTS AND DISCUSSION

Brønsted Acid-Catalyzed Oligomerization of Styrene Derivatives as Single Molecule Probe Reaction. Previous studies of the styrene oligomerization reaction suggested a reaction mechanism for the formation of fluorescent carbocationic species,[29,30,64−66] as outlined in Scheme 1. Upon protonation of the neutral styrene molecule (**1**), the

Scheme 1. Potential Reaction Pathways and Species Proposed for the Oligomerization of Styrene Derivatives, In Particular 4-Methoxystyrene and 4-Fluorostyrene, in Acidic Zeolites[29,30,64,66a]

^{a}The absorption maxima for the species (**5−7**) represent the experimentally observed absorption bands shown in Supporting Information Figure S1.

initial benzylic carbocation (**2**) is formed. Further dimerization leads to the formation of the linear dimeric 1,3-bis(phenyl)-1-butylium cation (**3**), that can transform into neutral diphenyl alkene upon proton transfer to the zeolite framework (**4**), or undergo cyclization to the cyclic dimeric 3-methyl-1,4-phenyl-indanyl (indanyl) carbocation (**7**). The formation of the linear allylic carbocation (**5**) has been the subject of particular interest due to its photoproperties. According to Cozens et al.,[64] and Buurmans et al.,[66] molecules (**3**) and (**4**) can undergo bimolecular hydride transfer to form an allylic carbocation (**5**). The conjugated carbocations (**5**) and (**7**) are reported in the literature as the stable carbocations that can absorb visible light. The absorption originating from the trimeric species (**6**) was previously proposed,[28,30] although its precise molecular structure is still unknown.

The absorption and emission properties of the 4-methoxystyrene and 4-fluorostyrene carbocations (**5**–**7**) under study were determined in a series of UV–vis and confocal fluorescence microscopy experiments, which are summarized in the Supporting Information Figures S1 and S2. The oligomerization of both probe molecules resulted in several absorption bands indicated in Scheme 1. The fluorescence spectra of H-ZSM-5 crystals exposed to 4-methoxystyrene exhibit two main emission bands at ~600 and 650 nm (Supporting Information Figure S2) that are assigned to the linear dimeric and trimeric species, respectively. Similar conclusions can be made with respect to the origin of the fluorescence bands observed for the 4-fluorostyrene oligomers. In this case, the corresponding emission bands were observed at ~580 and 640 nm. In what follows, we will use these spectroscopic assignments to explain the observations from our single molecule fluorescence microscopy measurements.

Single Molecule Fluorescence Microscopy Imaging of Crystalline Defects in Zeolite ZSM-5 Crystals. Under optimal conditions for single molecule imaging, the speed of fluorescent product disappearance due to photobleaching or migration out of focus should match the formation of novel fluorescent oligomers. The room temperature reaction in pure 4-methoxystyrene resulted in a very fast buildup of the fluorescence signal that could not be matched by the photobleaching induced by the excitation laser. Under such conditions, for the large majority of the crystals, the fast accumulation of overall fluorescence hampers the continuous detection of single fluorescent reaction products being formed. In this case, the reaction rate needs to be controlled by introducing a solvent, which will be discussed below. Notably, single molecule sensitivity could be reached in solvent-free conditions by studying H-ZSM-5 crystals with low Brønsted acidity, making use of the large interparticle differences in reactivity (Supporting Information Figure S3).

The localization of fluorescent reaction products that appeared as the result of stochastic catalytic turnovers was achieved by the Nanometer Accuracy by Stochastic Chemical reActions (NASCA) super-resolution fluorescence method. The method enables following real-time catalytic events taking place within a catalytic solid.[24] By using NASCA approach, the 4-methoxystyrene oligomerization was followed with a 30–100 ms temporal resolution and individual product molecules were localized using 2-D Gaussian fitting procedure with an estimated lateral resolution of about 20 nm (Supporting Information Figure S4). This is more than a 10-fold improvement of the diffraction-limited resolution and a remarkable improvement in sensitivity as compared to the

UV–vis and fluorescence microscopy studies reported previously.[30,67]

Figure 1 summarizes the results for a parent zeolite H-ZSM-5 crystal recorded in solvent-free conditions and at two different
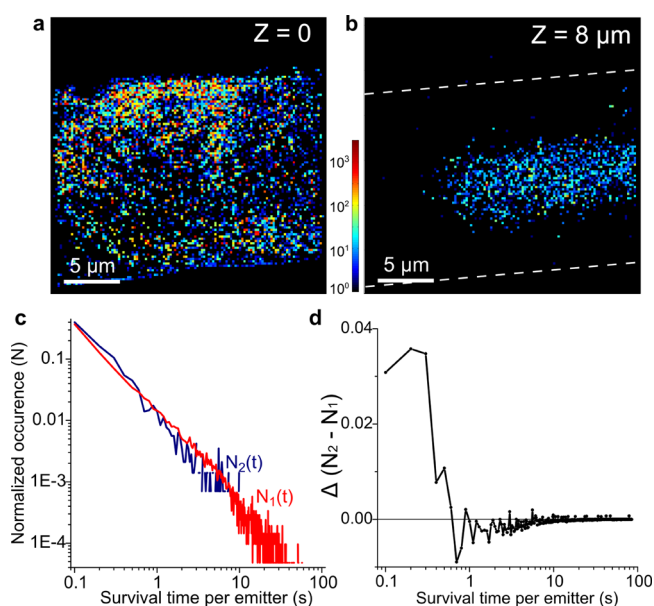

Figure 1. High-resolution single molecule fluorescence microscopy imaging of fluorescent reaction products recorded after 1 h during ~500 s of the solvent-free oligomerization of 4-methoxystyrene on a parent zeolite H-ZSM-5 crystal; the excitation wavelength was 561 nm. (a,b) Accumulated maps of the total number of detected fluorescent events counted separately in each of 5000 frames (color bar: number of events per 200×200 nm^2 presented on the logarithmic scale, noncorrected for repeated detection of single product molecules), (a) recorded in the near-surface region of the crystal and (b) recorded at $Z = 8$ μm from the surface and toward the middle of the crystal. The edges are not fluorescent due to the orientation of the product molecules with respect to the laser beam and light polarization. (c) Normalized occurrence of emitters with different survival times, calculated for the surface ($N_1(t)$, red) and $Z = 8$ μm ($N_2(t)$, blue). (d) The difference in normalized occurrences for the distributions in (c).

focal depths—at the zeolite surface (Figure 1a, $Z = 0 \pm 0.2$ μm) and in the middle of the zeolite crystal (Figure 1b, $Z = 8$ μm). The reconstructed high-resolution maps in Figure 1a,b present the total number of detected single emitting molecules, accumulated independently over 5000 frames (≈ 500 s). At the surface, fluorescent reaction product molecules cluster in certain regions (Figure 1a), whereas at the middle of the crystal ($Z = 8$ μm) an active region with more evenly distributed fluorescence events is present (Figure 1b). The scatter plots of individual localizations support this conclusion (Supporting Information Figure S4). The low surface reactivity of the studied parent H-ZSM-5 crystal (as compared to the more reactive crystals) points to the acid site inaccessibility due to the extremely high and inhomogeneous surface diffusion resistance caused by zeolite pore blockage.[13,15]

An important observation from Figure 1a is that a high number of fluorescent events can be detected in the yellow/red color-coded crystalline domains. Inspection of the recorded fluorescent movie (Supporting Information Movie S1) reveals high fluorescence movie activity in these regions. Highly photostable fluorescent emitters were found to contribute about 25% to the observed fluorescence activity. To confirm

this observation we have analyzed the photostability of the individual fluorescent reaction products. A particle-tracking algorithm was applied to account for reappearing individual fluorescent molecules within certain spatial and temporal constrains.[26] Based on the analysis described in Supporting Information Figure S5, we considered that the consecutive localizations within ~60 nm distance originate from the same molecule; additionally, the blinking dark states (off times) in duration shorter than 2 s were considered to originate from the same molecule. These values were found to represent well the reappearance of the highly photostable emitters.

By using determined localization values, we have examined the survival times of fluorescent 4-methoxystyrene oligomers for both studied cases in Figure 1a and b, respectively. Figure 1c summarizes the normalized distributions of survival times for the fluorescent molecules at the surface ($N_1(t)$) and at $Z = 8$ μm ($N_2(t)$). We detect a broad range of survival times for fluorescent emitters, covering 3 orders of magnitude from 100 ms to 50 s. The difference (Δ) between the normalized distributions $N_2(t) - N_1(t)$ is shown in Figure 1d. The result indicates that the fraction of molecules with the lower survival times ($\leq$700 ms) is higher for the movie recorded at $Z = 8$ μm, whereas the movie recorded at the surface of the parent zeolite H-ZSM-5 crystal has a higher contribution of the highly photostable emitters (survival times > 700 ms), Supporting Information Movie S1.

The measured differences in the survival times of fluorescent products suggest the formation of fluorescent species with different photostability. The linear dimeric carbocations (**5**) form easily in the zeolite micropores and under highly diluted conditions they should be the predominant species. The trimeric (**6**) and cyclic dimeric (**7**) carbocations are likely to be formed at more accessible acid sites close to the zeolite outer surface. Defects in the crystalline structure may facilitate further oligomerizations in larger voids where the local porous environment does not induce severe shape constraints.[30,66,68] The formation of the trimeric carbocation species (**6**) seems to be kinetically controlled and follows the formation of the linear dimeric carbocation species (**5**),[28] as evidenced from Scheme 1 and the UV–vis spectroscopy experiments (Supporting Information Figure S3). In the single molecule fluorescence microscopy experiments we have used 532 and 561 nm nm laser excitation, meaning that we simultaneously excite both the linear dimeric (**5**) (emission at 600 nm) and the trimeric species (**6**) (emission at 650 nm). Therefore, the formation of the photostable trimeric fluorescent products close to the surface could explain the observed differences in survival times of individual emitters. The high stability of the trimeric species is most probably related to their low reactivity, as further oligomerization is unlikely to happen.

After applying the correction for the reappearance of individual molecules, it was possible to construct super-resolution NASCA reactivity maps by binning individual catalytic turnovers in 200 × 200 nm^2 areas. To distinguish between dimeric and trimeric species, we have chosen a threshold value for survival times of 0.7 s. Note that this arbitrary threshold value, as determined from Figure 1d, will be only used to illustrate the concept of distinguishing fluorescent species with different lifetimes. In Figure 2, we have spatially resolved the appearance of trimeric fluorescent molecules (survival times > 0.7 s) and dimeric fluorescent molecules (survival times ≤ 0.7 s). The dimeric species are formed both at the surface and in the middle of a zeolite crystal (Figure 2a,c),
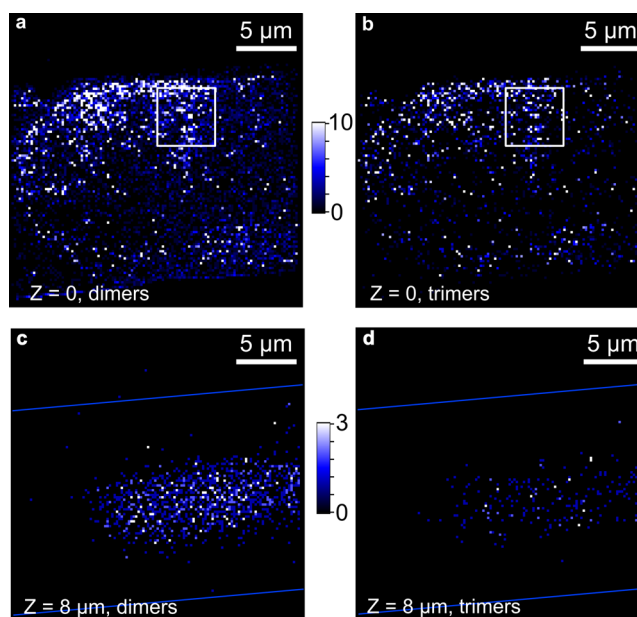

Figure 2. High-resolution single molecule fluorescence microscopy maps of the short-lived (<0.7s; dimeric) and long-lived (>0.7s; trimeric) species, reconstructed based on the survival times of fluorescent molecules shown in Figure 1a,b. (a−d) Accumulated maps of (a) dimeric products at the outer surface of the crystal, (b) trimeric products at the outer surface of the crystal, (c) dimeric products at $Z = 8$ μm, and (d) trimeric products at $Z = 8$ μm. The white squares indicate the region of interest magnified in Figure 3a. Color scale bars denote a total number of dimeric and trimeric emitters per 200 × 200 nm^2 detected during 500 s.

whereas the trimeric species were predominantly detected close to the outer surface of the zeolite H-ZSM-5 crystal (Figure 2b,d).

Our interpretation can be further supported by inspecting the nanoscopic regions of interest, such as the region highlighted in Figure 2a,b and presented as a scatter plot of fluorescent events in Figure 3a. We represent the dimeric and trimeric fluorescent species by the blue and red circles, respectively. Qualitatively, the highly photostable events (in red) seem to appear in agglomerates and in close proximity to each other. The less photostable dimeric species (in blue) appear more evenly distributed within the analyzed region. A similar conclusion can be made for the entire maps of dimeric and trimeric species presented in Figure 2a,b. This is a clear indication that the two types of fluorescent reaction products are formed in conditions of different accessibility of acid sites. Consequently, the local reactivity rates and the kinetics of dimer/trimer formation are largely determined by the accessible Brønsted acid sites.

The spatial arrangement of the dimeric and trimeric fluorescent species can be quantified by calculating the nearest neighbor distances for both types of the formed products. The results are shown in Figure 3b for both short-lived (dimeric) and long-lived (trimeric) species. A clear distinction can be made between the distributions of NN distances. Both distributions show a maximum number of counts for the very short NN distances (<25 nm). A close inspection of the scatter plot in Figure 3a confirms that these localizations predominantly originate from clustered events, where the formation of both dimeric and trimeric species is facilitated. It is not possible to make a clear distinction between both reaction products at
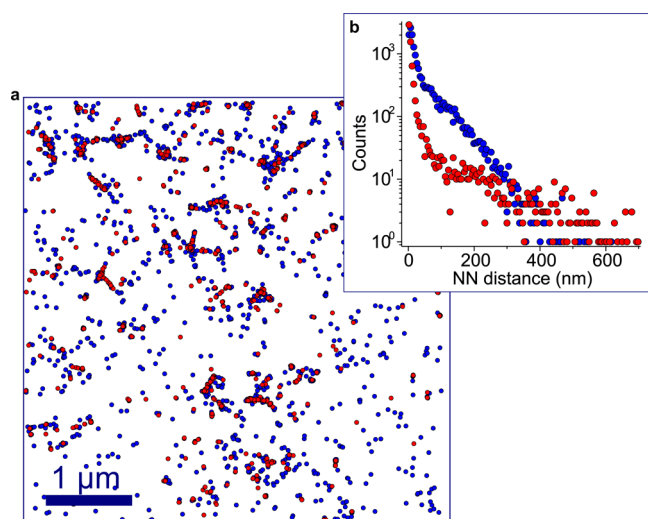
Figure 3. Nearest neighbor (NN) analysis for the formation of the dimeric (blue) and trimeric fluorescent species (red). (a) Scatter plot of the fluorescent products. (b) Frequency of the NN distances for the dimeric (blue) and trimeric carbocations (red) calculated for the entire data set presented in Figure 2.

evenly formed throughout the microporous crystalline domains, as qualitatively presented in Figure 2.

The presented analytical approach offers a possibility to study defect-induced chemistry of zeolite ZSM-5 by following two distinct types of fluorescent species. The working hypothesis was further tested by deliberately inducing structural defects into the zeolite framework by dealumination of the parent zeolite H-ZSM-5 crystals via mild steaming at 773 K. 4-Methoxystyrene appeared to be very sensitive to the induced crystalline defects. The reactivity of parent and steamed zeolite H-ZSM-5 crystals were compared in a series of concentration experiments with a 4-methoxystyrene solution in *n*-heptane.

As discussed earlier, the exposure of the parent H-ZSM-5 crystals to liquid (nondiluted) 4-methoxystyrene leads to the fast accumulation of fluorescence where single fluorescent reaction products cannot be resolved anymore, as illustrated in Figure 4a. Significant dilution of 4-methoxystyrene in heptane (7.4 mM) was necessary to observe well-separated and localized fluorescent reaction products in such active parent H-ZSM-5 crystals (Figure 4b). Reducing the concentration of 4-methoxystyrene also slows down the intracrystalline diffusion with fluorescent oligomers predominantly detected near the zeolite surface (~0.5 μm). As expected, the reactivity decreased for more than 1 order of magnitude when the crystals were exposed to a 1.5 mM 4-methoxystyrene solution (Figure 4c). In both cases, the individual single molecule products could be clearly resolved by the localization algorithm (red circles in Figure 4). However, when the steamed H-ZSM-5 crystals were exposed to a 1.5 mM 4-methoxystyrene solution, an overwhelming amount of fluorescent carbocation products was detected making it impossible to efficiently resolve individual molecules (Figure 4e). Reducing the concentration 10-fold did not resolve this problem (Figure 4f); only further 50-fold dilution of 4-methoxystyrene to 30 μM made it possible to observe isolated fluorescent species (Figure 4g).
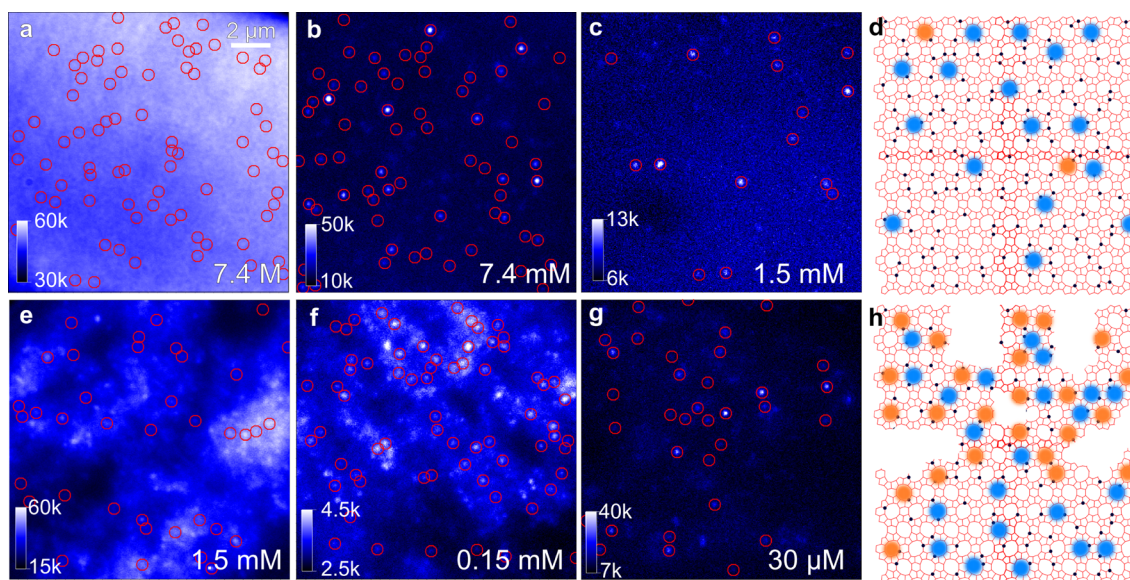
distances that are below the resolution limit as the optimized parameters of localization are arbitrary and cannot exclude the blinking of individual molecules and statistical distribution in survival times of fluorescent products. Therefore, within this resolution limit, the measured numbers should be seen as a semiquantitative description of the NN distances. However, the dimeric species show also a considerable fraction of NN distances that are in the range of 100−300 nm (Figure 3b), values that are well above the resolution limit. This is expected from the initial assumption that the dimeric species are more

Figure 4. Probing the accessibility of parent (top) and steamed zeolite H-ZSM-5 crystals (bottom). Wide-field fluorescence micrographs of the Brønsted acid-catalyzed oligomerization of 4-methoxystyrene at different molar concentrations in heptane (bottom right); images are recorded at the surface of the parent (a−c) and steamed (e−g) zeolite H-ZSM-5 crystals by using a 532 nm excitation; (a) was measured in solvent-free conditions (7.4 M). The red circles indicate the efficiency of the localization algorithm to detect individual fluorescent events. (d, h) Cartoons illustrating the formation of dimeric and trimeric fluorescent species in parent (d) and steamed (h) zeolite H-ZSM-5 crystals. The light blue dots indicate the formation of linear dimeric carbocations, while the red dots represent the bulkier trimeric carbocations, formed close to defects/mesopores.
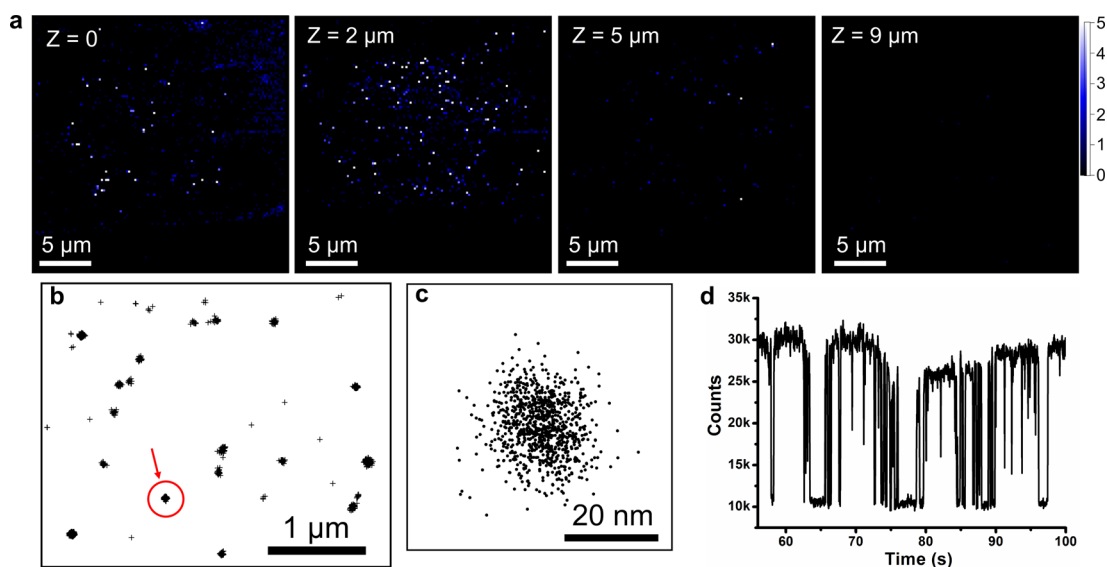
Figure 5. High-resolution fluorescence microscopy imaging of defect-induced reactivity of 4-methoxystyrene in a steamed H-ZSM-5 crystal, recorded in 30 μM solution in heptane by using a 532 nm excitation with 30 ms acquisition time. (a) Accumulated images of photoactivity for different focal depths denoted in the top left corner, recorded after ~1 h from the start of the reaction. The color scale bar represents the number of detected fluorescent styrene oligomers per 200×200 nm^2 during 150 s of the recording time. (b) High resolution scatter plot indicating the location of fluorescent products formed in a steamed zeolite H-ZSM-5 crystal at $Z = 2 \pm 0.3$ μm. (c,d) Corresponding (c) scatter plot and (d) fluorescence intensity trajectory of the single molecule indicated with the red arrow in (b). The background intensity in (d) is around 10k.

Our previous work has shown that the measured turnover frequencies of the parent and mildly steamed H-ZSM-5 crystals differ by a factor of 2−5.[26] The variation in fluorescence response with styrene derivatives is hence probably related to the formation of different, more photostable oligomers at the crystal defects giving rise to a pronounced increase in background fluorescence, as postulated earlier in the text. Spectroscopic evidence for this conclusion can be found by UV−vis microscopy. Two distinct absorption bands initially appear for both types of zeolite H-ZSM-5 crystals at ~565 and 590 nm (Supporting Information Figure S3). We attribute these absorption bands to the existence of two isomers of the allylic dimeric carbocation (**5**). The absorption bands at 490, 530, and 640 nm appear later in the spectrum, but faster on steamed zeolite H-ZSM-5 crystals and parent crystals with visible crystalline defects (Supporting Information Figure S3). Similar absorption profiles were reported previously.[28,64,65] The absorption band at ~640 nm has been attributed to the trimeric carbocationic species (**6**).[28,67] Despite the lack of evidence for their precise molecular structure(s), the extent of conjugation and late appearance of these species supports their assignment to the trimeric carbocationic species. The additional non-radiative relaxation pathways and energy transfer between the different fluorescent species are expected to be minimized in highly diluted solutions of the reactant and large product-to-product distances—conditions that are met in our experiments.

The observed behavior underlines the importance of pore accessibility and the shape-selective role of framework in the formation of bulkier reaction products. For instance, the highly crystalline parent zeolite H-ZSM-5 crystals typically have a Si-rich layer of up to 100 nm in thickness, that is characterized by a very low acid site density (Si/Al ratio of ~160).[59,61] This layer also seems to act as a shape-selective surface diffusion barrier hindering the formation of the bulkier fluorescent products at the very surface, as depicted in Figure 4d. The local diffusion properties are drastically changed with the formation of larger mesoporous defects,[11] which can facilitate the formation of

bulkier oligomers that are apparently more photostable (red dots depicted in Figure 4h).

The low concentrations of 4-methoxystyrene that are used in the experiments (<1 mM) favor the predominant formation of the linear dimeric carbocations in the micropores. Considering the high density of Brønsted acid sites, the formation of the highly photostable trimeric carbocationic species can be used to selectively probe more accessible Brønsted acid sites at the crystalline defects. A significant fraction of the parent zeolite crystals appeared to have intracrystalline defects (Supporting Information Figure S6), such as cracks and mesoporous defects, which are inherent to the sample preparation, such as synthesis, activation and calcination. Notably, the important role of crystalline defects in base-leaching of zeolite H-ZSM-5 was reported recently on nanosized zeolite H-ZSM-5 crystals, making the single molecule visualization of the defects a very relevant topic for zeolite chemistry.[16,17] In a similar fashion, the developed method can be used to qualitatively visualize interparticle differences in the uptake of probe molecules. These become obvious for the steamed zeolite H-ZSM-5 crystals where different crystals can have strikingly different reactivity (Supporting Information Figure S6). We speculate that the interparticle differences arise due to structural heterogeneities, such as amorphous deposition or framework distortions that may strongly influence local surface mass transport and reactivity.[69]

The selective formation of trimeric carbocations can be maximized in the conditions of extremely low concentration of the selected styrene derivatives. The high-resolution maps of a steamed H-ZSM-5 crystal, measured at four different focal depths, are shown in Figure 5a. The majority of the photostable reaction products were formed in a 2−3 μm thick surface layer of the zeolite crystal (Supporting Information Movie S2). Previous high-resolution SEM studies of steamed zeolite H-ZSM-5 crystals detected near-surface mesopores with diameters of 5−50 nm. However, almost no damage of the crystalline structure (i.e., mesoporosity) was observed in H-ZSM-5 crystals
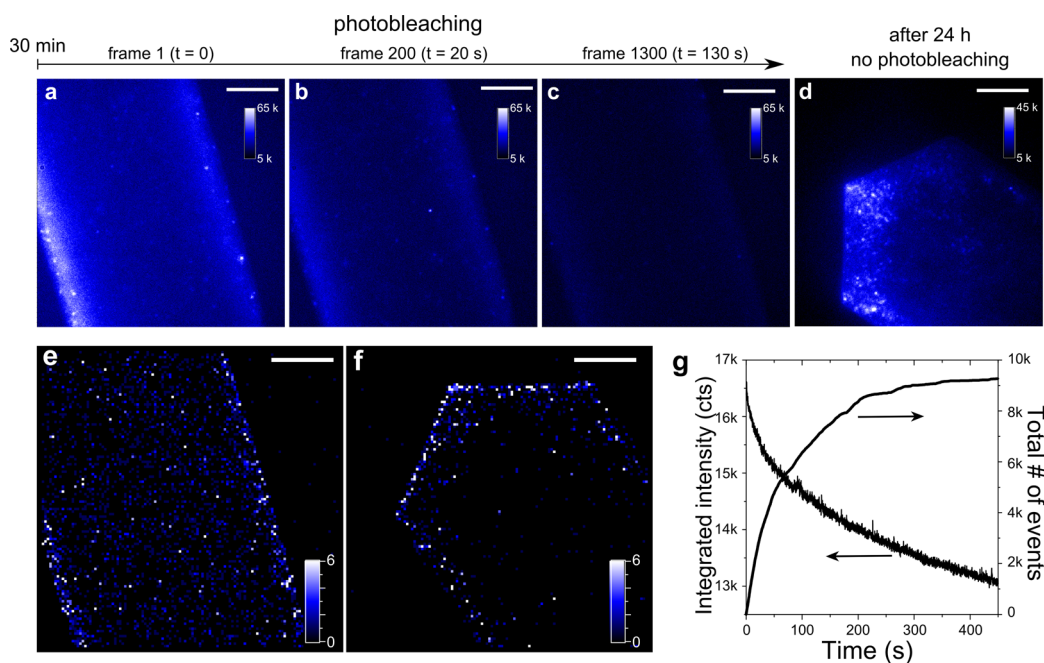
Figure 6. Oligomerization of 4-methoxystyrene (2.5 M in 1-butanol) at parent zeolite H-ZSM-5 crystals. (a−c) Wide-field fluorescence micrographs recorded 30 min after start of the reaction by using a 561 nm excitation. The sequence illustrates the effect of photobleaching, (a) at the beginning of recording, (b) after 20 s, and (c) after 130 s; (d) recorded after 24 h, at Z = 4 μm. (e,f) Accumulated high-resolution reactivity maps recorded at (e) the middle of the zeolite crystal, (f) the edge of the zeolite crystal. (g) Integrated total fluorescence background intensity and the number of detected fluorescent events, as measured for the crystal in (f). Color scale bars denote the total number of turnovers per 200 × 200 nm^2 detected during 500 s. Acquisition time in (a−d) was 100 ms. Scale bars are 5 μm.

further away from the outer surface.[60,61] This observation is in accordance with the 3-D reactivity profiles of furfuryl alcohol in the steamed zeolite H-ZSM-5.[26] Therefore, it is reasonable to suggest that the photostable emitters in Figure 5 reveal the locations of the accessible mesopores. Even though the concentration of 4-methoxystyrene in this experiment (30 μM) corresponds to only 17 molecules per 100 nm^3 of solvent, the kinetics of the product formation is elevated in mesopores by specific local adsorption and diffusion pathways. At Z = 2 μm below the zeolite surface, a higher number of photostable and highly localized fluorescent oligomers was detected (Figure 5b). The detected emitters did not show significant diffusion and consecutive localizations are within the localization precision of our method (~20 nm), as shown in Figure 5c. The recorded fluorescent reaction products show high photostability with occasional blinking, as evidenced from their fluorescence intensity trajectories (Figure 5d). By using single molecule fluorescence microscopy with 30 ms acquisition time it is possible to track the temporal changes in fluorescence for every individual fluorescent product. Several representative fluorescence intensity trajectories are presented in Supporting Information Figure S7.

The Effect of Solvent Polarity on the Oligomerization Reaction. In attempt to optimize the reaction rates for the highly reactive 4-methoxystyrene, we have tested the oligomerization reaction in 1-butanol. Whereas 4-methoxystyrene reacted readily at the Brønsted acid sites in a 1.5 mM (0.02 vol %) solution in n-heptane, hardly any fluorescent events were observed in a highly concentrated 2.5 M (33.3 vol %) solution in 1-butanol. The spatial reactivity distribution was clearly different with respect to n-heptane, with extremely low reactivity mostly observed at the edges of the H-ZSM-5 crystals (Figure 6a).

The initial fluorescence signal, recorded 30 min after initiating the reaction, vanished after 130 s of continuous illumination due to fast photobleaching of individual fluorescent molecules (Figure 6a−c). After 24 h, we observed significant penetration and accumulation of the fluorescent oligomers along the sinusoidal pores of the zeolite H-ZSM-5 crystal tips, also in the deeper regions of the crystals (Figure 6d). The observed reactivity and directionality of the fluorescent products in 1-butanol is a result of anisotropic diffusivity and reactivity of 4-methoxystyrene along the straight and sinusoidal channels. Kox et al. reported higher accessibility of the tip regions via the straight pores (running along the b lattice parameter) open to the surface, as illustrated in Supporting Information Figure S2.[28] The fluorescence response can be described in terms of low single molecule reactivity presented in Figure 6e and f; the analysis of the average fluorescence background signal and the number of detected fluorescent events showed that both quantities decayed fast in time (Figure 6g). We concluded that the rate of the oligomerization reaction in 1-butanol was very low and that only the initially formed fluorescent products were photobleached.

The change in the reaction medium affects not only the reactivity, but also the survival times of fluorescent products. The analysis of the survival times of the 4-methoxystyrene-derived carbocationic species in n-heptane and 1-butanol is shown in Figure 7a. Although the total number of detected fluorescent events is 2 orders of magnitude higher for the fluorescent reaction products in n-heptane, the measured exponential decays of the survival time frequencies clearly indicate a lower photostability for the fluorescent reaction products in 1-butanol; all exponential time constants appeared to be smaller in the latter case.
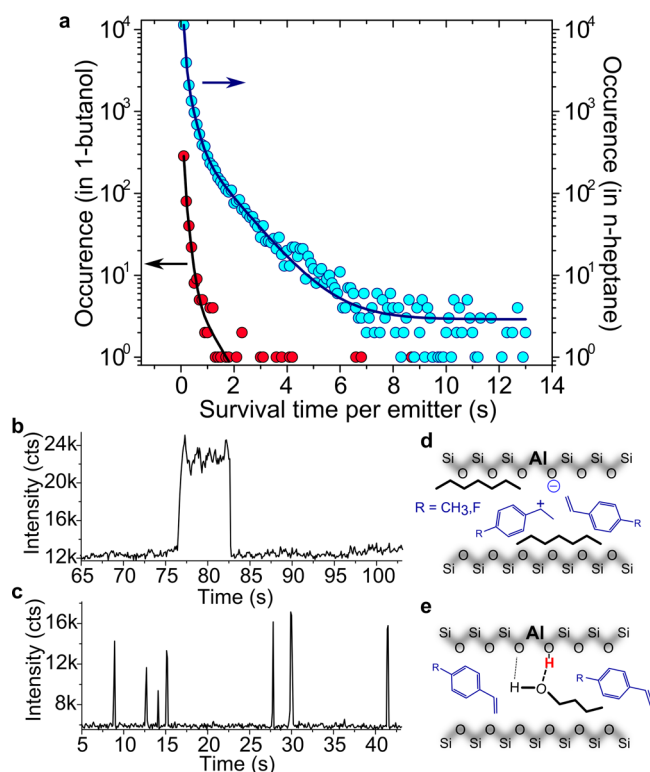
Figure 7. (a) Survival times of fluorescent reaction products during the oligomerization of 4-methoxystyrene with parent zeolite ZSM-5 crystals in 1-butanol (2.5 M, red circles) and *n*-heptane (7.4 mM, blue circles). Exponential time constants for the fits are 0.055 ± 0.001 s (27% contribution), 0.22 ± 0.01 s (45%), and 1.1 ± 0.1 s (28%) for the emitters in *n*-heptane (blue fit) and 0.015 ± 0.05 s (18%), 0.13 ± 0.01 s (64%) and 0.8 ± 0.2 s (18%) for the emitters in 1-butanol (black fit). Note the logarithmic scale on *y*-axes. (b,c) Examples of the fluorescence intensity trajectories of individual fluorescent molecules in (b) *n*-heptane and (c) 1-butanol. (d,e) Schematic of the styrene oligomerization reaction in (d) *n*-heptane and (e) 1-butanol; the interaction of a solvent molecule with a Brønsted acid site is highlighted.

By inspecting the fluorescence behavior of individual emitters, it is possible to give a more qualitative description of their interactions with the zeolite framework. In a parent zeolite crystal, the fluorescent reaction products are confined within the micropores and the measured survival times provide information about framework-emitter interactions. Manual inspection of a large number of individual fluorescence trajectories confirmed the results presented in Figure 7a. The fluorescent reaction products in *n*-heptane on average have longer survival times, as illustrated for the fluorescence intensity trajectory of an emitter in Figure 7b. In stark contrast, fluorescent reaction products in 1-butanol predominantly show short survival times, often within the acquisition time of 100 ms. This is illustrated in Figure 7c, where one fluorescence trajectory consists of several short intensity bursts possibly originating from one fluorescent molecule.

The experimentally observed results can be explained by the competing role of solvent molecules as they may adsorb on the Brønsted acid sites, as depicted in Figure 7d,e. The significant drop in the reaction rates and the photostability of individual fluorescent reaction products are due to the strong chemisorption of 1-butanol at Brønsted acid sites. This solvent is known to occupy 96% of the zeolite volume with about 2 molecules per acid site (measured for a Si/Al ratio of 72).[70] The close packing of 1-butanol molecules is due to their strong interaction with Brønsted acid sites, but also due to favorable interactions of the hydrocarbon chain with the zeolite wall (Figure 7e).[71] As a result, the formation and thermodynamic stability of the benzylic and dimeric carbocationic species is severely inhibited by the presence of the polar solvent molecules. Heptane, on the other hand, has a similar pore filling as 1-butanol for the same reasons of C−H/zeolite wall interactions,[72] but does not interact strongly with the Brønsted acid sites, which can additionally promote the formation of carbocationic species (Figure 7d). Similar tests in 1,4-dioxane did not yield any visible photoproducts. In line with our results, Yoon et al. have reported in their bulk experiments a full conversion of styrene in dichloromethane over zeolite H−Y powder, and no evidence of reaction in tetra-hydrofuran or acetonitrile.[73]

The Effect of the Para-Substituent on the Oligomerization Reaction. The presented single molecule fluorescence microscopy approach can be successfully extended to other substituted styrene probe molecules. In this way, a broad range of reaction conditions can be achieved considering the large difference in reactivity between differently substituted derivatives. The trends in reactivity, as determined by the stabilization of the initial benzylic carbocation, can be predicted by Hammett parameters.[74−76] In a comparative study, Stavitski et al. have shown that the presence of different functional groups may affect the net stabilization of the benzylic species.[29] For example, fluoro- substituent has less stabilizing effect than methoxy- group in the *para* position, resulting in the much lower reactivity of 4-fluorostyrene at room temperature. However, it should be noted that the reactivity trends in zeolites may strongly deviate from the Hammett equation, as the confinement effects may play important role.[29] The fluorescent reaction products for 4-fluorostyrene can be detected at room temperature by using single molecule fluorescence microscopy. Using this less-reactive probe molecule similar solvent effect is observed, whereas imaging of the crystalline interior is readily possible in solvent-free conditions (Supporting Information Figure S8).

Quantitative Comparison of the Oligomerization Rates. Single molecule fluorescence microscopy can be considered as a quantitative technique provided that conditions for efficient localization of fluorescent molecules are met. By quantifying the individual fluorescent reaction products it was possible to estimate the averaged turnover frequencies recorded in the studied oligomerization reactions. For simplicity we have considered each fluorescent event to be one catalytic turnover. The results are summarized in Figure 8. A concentration range for successful single molecule fluorescence imaging of zeolites will depend on the reactivity of a probe molecule (i.e, the substituent effect) and the polarity of a solvent (i.e., the solvent effect). In both cases the oligomerization rate is determined by the tendency of the reactant to form the initial benzylic and dimeric carbocations. The polarity of a solvent and its interaction with Brønsted acid sites plays a crucial role in the carbocation formation, as illustrated for the reactions in *n*-heptane and 1-butanol. The oligomerization of both reactants is significantly inhibited when *n*-heptane is replaced with 1-butanol (Figure 8a).

The oligomerization of 4-methoxystyrene in zeolite H-ZSM-5 proceeds much faster than in the case of 4-fluorostyrene, as visible from the comparison of their reactivity in heptane
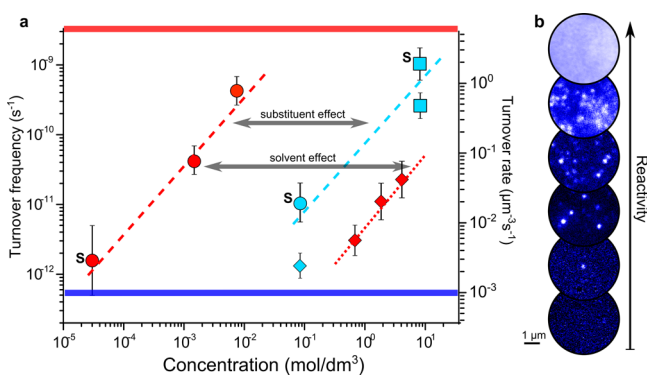
Figure 8. (a) Reactivity of 4-methoxystyrene (in red) and 4-fluorostyrene (in blue) as probe molecules for single molecule chemical imaging in *n*-heptane (circles) and 1-butanol (rhombi). The squares represent 99% pure 4-fluorostyrene. Averaged turnover frequencies of the parent and steamed zeolite H-ZSM-5 crystals (denoted as "S") were recorded close to the outer surface of the single crystals; *x*-axis denotes the concentration of the probe molecules in the solvents. The blue and red lines indicate the lowest and highest turnover rates that can be imaged by the presented single molecule approach. The linearity shown is provided only as a guidance for the observed trends in reactivity. (b) Frames indicating the density of the individual emitters and an approximate level of reactivity for corresponding turnover frequencies.

(Figure 8a). A successful single molecule fluorescence microscopy imaging of zeolite H-ZSM-5 crystals reacting with 4-methoxystyrene can be performed at a high dilution of the reactant (10^{-5}–10^{-2} M in *n*-heptane). In contrast, the experiments with 4-fluorostyrene can routinely be performed with the pure reagent (8.3 M) for at least 30 min, even for the highly acidic zeolite H-ZSM-5 crystals.

The maximum recorded rate of fluorescent reaction product formation is in the order 10 events per μm^3 s^{-1}. If all Al atoms are considered catalytically equally active, this number approximately translates into the turnover frequencies in the order of 10^{-8} s^{-1} (red line in Figure 8a). The low turnover numbers of 10^{-12} s^{-1} (blue line Figure 8a) indicate the detection rate of <0.01 events μm^{-3} s^{-1}. Based on the presented results, it is clear that a subset of the acid sites are probed with our approach and this number is determined by the frequency and density of detected fluorescent events (Figure 8b). The approach does not determine the total concentration of acid sites, but rather relies on the accurate comparison of reaction rates recorded in a certain time frame, which ultimately determine the rate constants in the low-concentration regimes.

CONCLUSIONS

By using single molecule fluorescence microscopy in combination with the selective oligomerization of styrene derivatives, we were able to visualize for the first time host- and guest-dependent proton transfer processes in zeolite ZSM-5 crystals at the single particle–single molecule level. The formation of linear dimeric and trimeric styrene carbocations, characterized by different photostabilities, can be used to selectively probe highly accessible acid sites at crystalline defects. Interestingly, the oligomerization rate was found to be very sensitive to changes in the polarity of the solvent medium and chemical nature of the *para*-substituent of the styrene moiety. Both changes lead to several orders of magnitude difference in reactivity of zeolite crystals. With this approach in

hand, we have established a probe concept that is very sensitive to chemical changes in the nature of the zeolite host as well as of the guest species and that is capable of resolving nanoscopic details in the reactivity of zeolite crystals with the ultimate single molecule sensitivity.

ASSOCIATED CONTENT

⊙ Supporting Information

The Supporting Information is available free of charge on the ACS Publications website at DOI: 10.1021/jacs.6b06083.

> Additional spectra and high-resolution images of intra- and interparticle heterogeneities, and single molecule fluorescence intensity trajectories (PDF)
>
> Photoactivity of a parent zeolite ZSM-5 crystal in 4-methoxystyrene (AVI)
>
> Reactivity of a steamed zeolite ZSM-5 crystal in 30 μM solution of 4-methoxystyrene in n-heptane (AVI)

AUTHOR INFORMATION

Corresponding Authors
*maarten.roeffaers@biw.kuleuven.be
*b.m.weckhuysen@uu.nl
Notes
The authors declare no competing financial interest.

ACKNOWLEDGMENTS

REFERENCES

(1) *Handbook of heterogeneous catalysis*; Ertl, G., Knozinger, H., Schüth, F., Weitkamp, J., Eds.; Wiley-VCH: Weinheim, 2008.
(2) *Zeolites and catalysis: synthesis, reactions and applications*; Čejka, J., Corma, A., Zones, S., Eds.; Wiley-VCH: Weinheim, 2010.
(3) Bellussi, G.; Carati, A.; Millini, R. Industrial potential of zeolites. In *Zeolites and catalysis: synthesis, reactions and applications*; Čejka, J., Corma, A., Zones, S., Eds.; Wiley-VCH: Weinheim, 2010; pp 449–491.
(4) Corma, A. Application of zeolites in fluid catalytic cracking and related processes. In *Studies in Surface Science and Catalysis. Zeolites: Facts, Figures, Future*; Jacobs, P. A., van Santen, R. A., Eds.; Elsevier: Amsterdam, 1989; Vol. 49, pp 49–67.
(5) Hagen, J. *Industrial Catalysis: A Practical Approach*; Wiley-VCH: Weinheim, 2005.
(6) Vogt, E. T. C.; Whiting, G. T.; Dutta Chowdhury, A.; Weckhuysen, B. M. *Adv. Catal.* **2015**, *58*, 143.
(7) Vogt, E. T. C.; Weckhuysen, B. M. *Chem. Soc. Rev.* **2015**, *44*, 7342.
(8) Jacobs, P. A.; Dusselier, M.; Sels, B. F. *Angew. Chem., Int. Ed.* **2014**, *53*, 8621.
(9) Mitchell, S.; Michels, N.-L.; Kunze, K.; Pérez-Ramírez, J. *Nat. Chem.* **2012**, *4*, 825.

(10) Mitchell, S.; Pinar, A. B.; Kenvin, J.; Crivelli, P.; Kärger, J.; Pérez-Ramírez, J. *Nat. Commun.* **2015**, *6*, 8633.

(11) van Donk, S.; Janssen, A. H.; Bitter, J. H.; de Jong, K. P. *Catal. Rev.: Sci. Eng.* **2003**, *45*, 297.

(12) Weckhuysen, B. M. *Angew. Chem., Int. Ed.* **2009**, *48*, 4910.

(13) Hibbe, F.; Chmelik, C.; Heinke, L.; Pramanik, S.; Li, J.; Ruthven, D. M.; Tzoulaki, D.; Kärger, J. *J. Am. Chem. Soc.* **2011**, *133*, 2804.

(14) Hibbe, F.; Caro, J.; Chmelik, C.; Huang, A.; Kirchner, T.; Ruthven, D.; Valiullin, R.; Kärger, J. *J. Am. Chem. Soc.* **2012**, *134*, 7725.

(15) Kärger, J.; Binder, T.; Chmelik, C.; Hibbe, F.; Krautscheid, H.; Krishna, R.; Weitkamp, J. *Nat. Mater.* **2014**, *13*, 333.

(16) Fodor, D.; Krumeich, F.; Hauert, R.; van Bokhoven, J. A. *Chem. - Eur. J.* **2015**, *21*, 6272.

(17) Fodor, D.; Beloqui Redondo, A.; Krumeich, F.; van Bokhoven, J. A. *J. Phys. Chem. C* **2015**, *119*, 5447.

(18) Buurmans, I. L. C.; Ruiz-Martínez, J.; Knowles, W. V.; van der Beek, D.; Bergwerff, J. A.; Vogt, E. T. C.; Weckhuysen, B. M. *Nat. Chem.* **2011**, *3*, 862.

(19) De Cremer, G.; Sels, B. F.; De Vos, D. E.; Hofkens, J.; Roeffaers, M. B. J. *Chem. Soc. Rev.* **2010**, *39*, 4703.

(20) Stavitski, E.; Weckhuysen, B. M. *Chem. Soc. Rev.* **2010**, *39*, 4615.

(21) Domke, K. F.; Riemer, T. A.; Rago, G.; Parvulescu, A. N.; Bruijnincx, P. C. A.; Enejder, A.; Weckhuysen, B. M.; Bonn, M. *J. Am. Chem. Soc.* **2012**, *134*, 1124.

(22) Kerssens, M. M.; Sprung, C.; Whiting, G. T.; Weckhuysen, B. M. *Microporous Mesoporous Mater.* **2014**, *189*, 136.

(23) Roeffaers, M. B. J.; Sels, B. F.; Uji-i, H.; Blanpain, B.; L'hoëst, P.; Jacobs, P. A.; De Schryver, F. C.; Hofkens, J.; De Vos, D. E. *Angew. Chem., Int. Ed.* **2007**, *46*, 1706.

(24) Roeffaers, M. B. J.; De Cremer, G.; Libeert, J.; Ameloot, R.; Dedecker, P.; Bons, A.-J.; Bückins, M.; Martens, J. A.; Sels, B. F.; De Vos, D. E.; Hofkens, J. *Angew. Chem., Int. Ed.* **2009**, *48*, 9285.

(25) Liu, K.-L.; Kubarev, A. V.; van Loon, J.; Uji-i, H.; De Vos, D. E.; Hofkens, J.; Roeffaers, M. B. J. *ACS Nano* **2014**, *8*, 12650.

(26) Ristanović, Z.; Hofmann, J. P.; De Cremer, G.; Kubarev, A. V.; Rohnke, M.; Meirer, F.; Hofkens, J.; Roeffaers, M. B. J.; Weckhuysen, B. M. *J. Am. Chem. Soc.* **2015**, *137*, 6559.

(27) Kox, M. H. F.; Mijovilovich, A.; Sättler, J. J. H. B.; Stavitski, E.; Weckhuysen, B. M. *ChemCatChem* **2010**, *2*, 564.

(28) Kox, M. H. F.; Stavitski, E.; Weckhuysen, B. M. *Angew. Chem., Int. Ed.* **2007**, *46*, 3652.

(29) Stavitski, E.; Kox, M. H. F.; Weckhuysen, B. M. *Chem. - Eur. J.* **2007**, *13*, 7057.

(30) Sprung, C.; Weckhuysen, B. M. *J. Am. Chem. Soc.* **2015**, *137*, 1916.

(31) Lu, H. P.; Xun, L.; Xie, X. S. *Science* **1998**, *282*, 1877.

(32) Tinnefeld, P.; Sauer, M. *Angew. Chem., Int. Ed.* **2005**, *44*, 2642.

(33) Wöll, D.; Braeken, E.; Deres, A.; De Schryver, F. C.; Uji-i, H.; Hofkens, J. *Chem. Soc. Rev.* **2009**, *38*, 313.

(34) Cordes, T.; Blum, S. A. *Nat. Chem.* **2013**, *5*, 993.

(35) Chen, P.; Zhou, X.; Shen, H.; Andoy, N. M.; Choudhary, E.; Han, K.-S.; Liu, G.; Meng, W. *Chem. Soc. Rev.* **2010**, *39*, 4560.

(36) Tachikawa, T.; Majima, T. *Chem. Soc. Rev.* **2010**, *39*, 4802.

(37) Buurmans, I. L. C.; Weckhuysen, B. M. *Nat. Chem.* **2012**, *4*, 873.

(38) Janssen, K. P. F.; De Cremer, G.; Neely, R. K.; Kubarev, A. V.; van Loon, J.; Martens, J. A.; De Vos, D. E.; Roeffaers, M. B. J.; Hofkens, J. *Chem. Soc. Rev.* **2014**, *43*, 990.

(39) Rybina, A.; Lang, C.; Wirtz, M.; Grußmayer, K.; Kurz, A.; Maier, F.; Schmitt, A.; Trapp, O.; Jung, G.; Herten, D.-P. *Angew. Chem., Int. Ed.* **2013**, *52*, 6322.

(40) Zhang, Y.; Song, P.; Fu, Q.; Ruan, M.; Xu, W. *Nat. Commun.* **2014**, *5*, 4238.

(41) Tian, Y.; Kuzimenkova, M. V.; Xie, M.; Meyer, M.; Larsson, P.-O.; Scheblykin, I. G. *NPG Asia Mater.* **2014**, *6*, e134.

(42) Tachikawa, T.; Majima, T. *J. Am. Chem. Soc.* **2009**, *131*, 8485.

(43) Sambur, J. B.; Chen, T.-Y.; Choudhary, E.; Chen, G.; Nissen, E. J.; Thomas, E. M.; Zou, N.; Chen, P. *Nature* **2016**, *530*, 77.

(44) Zürner, A.; Kirstein, J.; Döblinger, M.; Bräuchle, C.; Bein, T. *Nature* **2007**, *450*, 705.

(45) De Cremer, G.; Roeffaers, M. B. J.; Bartholomeeusen, E.; Lin, K.; Dedecker, P.; Pescarmona, P. P.; Jacobs, P. A.; De Vos, D. E.; Hofkens, J.; Sels, B. F. *Angew. Chem., Int. Ed.* **2010**, *49*, 908.

(46) Hutchison, J. A.; Uji-i, H.; Deres, A.; Vosch, T.; Rocha, S.; Müller, S.; Bastian, A. A.; Enderlein, J.; Nourouzi, H.; Li, C.; Herrmann, A.; Müllen, K.; De Schryver, F.; Hofkens, J. *Nat. Nanotechnol.* **2014**, *9*, 131.

(47) Su, L.; Lu, G.; Kenens, B.; Rocha, S.; Fron, E.; Yuan, H.; Chen, C.; Van Dorpe, P.; Roeffaers, M. B. J.; Mizuno, H.; Hofkens, J.; Hutchison, J. A.; Uji-i, H. *Nat. Commun.* **2015**, *6*, 6287.

(48) Roeffaers, M. B. J.; Sels, B. F.; Uji-i, H.; De Schryver, F. C.; Jacobs, P. A.; De Vos, D. E.; Hofkens, J. *Nature* **2006**, *439*, 572.

(49) Xu, W.; Kong, J. S.; Yeh, Y.-T. E.; Chen, P. *Nat. Mater.* **2008**, *7*, 992.

(50) Han, K. S.; Liu, G.; Zhou, X.; Medina, R. E.; Chen, P. *Nano Lett.* **2012**, *12*, 1253.

(51) Andoy, N. M.; Zhou, X.; Choudhary, E.; Shen, H.; Liu, G.; Chen, P. *J. Am. Chem. Soc.* **2013**, *135*, 1845.

(52) Ristanović, Z.; Kerssens, M. M.; Kubarev, A. V.; Hendriks, F. C.; Dedecker, P.; Hofkens, J.; Roeffaers, M. B. J.; Weckhuysen, B. M. *Angew. Chem., Int. Ed.* **2015**, *54*, 1836.

(53) Kubarev, A. V.; Janssen, K. P. F.; Roeffaers, M. B. J. *ChemCatChem* **2015**, *7*, 3646.

(54) Corma, A.; García, H. *J. Chem. Soc., Dalton Trans.* **2000**, *9*, 1381.

(55) Mores, D.; Stavitski, E.; Verkleij, S. P.; Lombard, A.; Cabiac, A.; Rouleau, L.; Patarin, J.; Simon-Masseron, A.; Weckhuysen, B. M. *Phys. Chem. Chem. Phys.* **2011**, *13*, 15985.

(56) Buurmans, I. L. C.; Ruiz-Martínez, J.; van Leeuwen, S. L.; van der Beek, D.; Bergwerff, J. A.; Knowles, W. V.; Vogt, E. T. C.; Weckhuysen, B. M. *Chem. - Eur. J.* **2012**, *18*, 1094.

(57) Karreman, M. A.; Buurmans, I. L. C.; Geus, J. W.; Agronskaia, A. V.; Ruiz-Martínez, J.; Gerritsen, H. C.; Weckhuysen, B. M. *Angew. Chem., Int. Ed.* **2012**, *51*, 1428.

(58) Karreman, M. A.; Buurmans, I. L. C.; Agronskaia, A. V.; Geus, J. W.; Gerritsen, H. C.; Weckhuysen, B. M. *Chem. - Eur. J.* **2013**, *19*, 3846.

(59) Karwacki, L.; Kox, M. H. F.; Matthijs de Winter, D. A.; Drury, M. R.; Meeldijk, J. D.; Stavitski, E.; Schmidt, W.; Mertens, M.; Cubillas, P.; John, N.; Chan, A.; Kahn, N.; Bare, S. R.; Anderson, M.; Kornatowski, J.; Weckhuysen, B. M. *Nat. Mater.* **2009**, *8*, 959.

(60) Karwacki, L.; de Winter, D. A. M.; Aramburo, L. R.; Lebbink, M. N.; Post, J. A.; Drury, M. R.; Weckhuysen, B. M. *Angew. Chem., Int. Ed.* **2011**, *50*, 1294.

(61) Aramburo, L. R.; Karwacki, L.; Cubillas, P.; Asahina, S.; de Winter, D. A. M.; Drury, M. R.; Buurmans, I. L. C.; Stavitski, E.; Mores, D.; Daturi, M.; Bazin, P.; Dumas, P.; Thibault-Starzyk, F.; Post, J. A.; Anderson, M. W.; Terasaki, O.; Weckhuysen, B. M. *Chem. - Eur. J.* **2011**, *17*, 13773.

(62) Dedecker, P.; Duwé, S.; Neely, R. K.; Zhang, J. *J. Biomed. Opt.* **2012**, *17*, 126008.

(63) Sergé, A.; Bertaux, N.; Rigneault, H.; Marguet, D. *Nat. Methods* **2008**, *5*, 687.

(64) Cozens, F. L.; Bogdanova, R.; Régimbald, M.; García, H.; Martí, V.; Scaiano, J. C. *J. Phys. Chem. B* **1997**, *101*, 6921.

(65) Fornés, V.; García, H.; Martí, V.; Fernández, L. *Tetrahedron* **1998**, *54*, 3827.

(66) Buurmans, I. L. C.; Pidko, E. A.; de Groot, J. M.; Stavitski, E.; van Santen, R. A.; Weckhuysen, B. M. *Phys. Chem. Chem. Phys.* **2010**, *12*, 7032.

(67) Kox, M. H. F.; Stavitski, E.; Groen, J. C.; Pérez-Ramírez, J.; Kapteijn, F.; Weckhuysen, B. M. *Chem. - Eur. J.* **2008**, *14*, 1718.

(68) Aramburo, L. R.; Wirick, S.; Miedema, P. S.; Buurmans, I. L. C.; de Groot, F. M. F.; Weckhuysen, B. M. *Phys. Chem. Chem. Phys.* **2012**, *14*, 6967.

(69) Remi, J. C. S.; Lauerer, A.; Chmelik, C.; Vandendael, I.; Terryn, H.; Baron, G. V.; Denayer, J. F. M.; Kärger, J. *Nat. Mater.* **2015**, *15*, 401.

(70) Aronson, M. T.; Gorte, R. J.; Farneth, W. E.; White, D. *Langmuir* **1988**, *4*, 702.

(71) Nguyen, C. M.; Reyniers, M.-F.; Marin, G. B. *Phys. Chem. Chem. Phys.* **2010**, *12*, 9481.

(72) Olson, D. H.; Kokotailo, G. T.; Lawton, S. L.; Meier, W. M. *J. Phys. Chem.* **1981**, *85*, 2238.

(73) Yoon, K. B.; Lim, J. L.; Kochi, J. K. *J. Mol. Catal.* **1989**, *52*, 375.

(74) Hammett, L. P. *J. Am. Chem. Soc.* **1937**, *59*, 96.

(75) Hansch, C.; Leo, A.; Taft, R. W. *Chem. Rev.* **1991**, *91*, 165.

(76) Leffler, J. E., Grunwald, E. *Rates and Equilibria of Organic Reactions*; Wiley: New York, 1963.